Microfluid Nanofluid (2009) 7:621–631
DOI 10.1007/s10404-009-0418-5

RESEARCH PAPER

Coupled solid (FVM)–fluid (DSMC) simulation of micro-nozzle with unstructured-grid

Zhi-Xin Sun · Zeng-Yao Li · Ya-Ling He · Wen-Quan Tao

Received: 2 December 2008 / Accepted: 30 January 2009 / Published online: 3 March 2009

Abstract The flow field and temperature distributions of free molecular micro-electro-thermal resist jet (FMMR) were studied resorting to DSMC–FVM coupled method. Direct simulation Monte Carlo (DSMC) method is the most useful tool to simulate the flow field of FMMR and unstructured grid is suitable for the flow simulation in a complicated region with tilted wall surface. DSMC code based on unstructured grid system was developed and the result was compared with that of structured grid and analytical solution to validate the reliability of the developed code. The DSMC method was then used to simulate the fluid flow in the micro-nozzle ($Kn > 0.01$) and the temperature distribution in the nozzle wall was obtained by the finite volume method (FVM). The Dirichlet–Neumann method was used to couple the wall heat flux and temperature between flow field and solid area. The effect of different income pressure was studied in detail and the results showed that the temperature of solid area changed drastically at different income pressure, so the commonly-adopted method of pre-setting boundary temperature before simulation was unreasonable.

Keywords FVM–DSMC coupled method · Unstructured-grid · FMMR

Z.-X. Sun · Z.-Y. Li · Y.-L. He · W.-Q. Tao (✉)
State Key Laboratory of Multiphase Flow in Power Engineering, School of Energy and Power Engineering, Xi'an Jiaotong University, 710049 Xi'an, Shaanxi, People's Republic of China
e-mail: wqtao@mail.xjtu.edu.cn

1 Introduction

Studies on small satellites or micro satellites are developed very fast recently for the advantage of small size, low cost and timesaving in manufacturing, and the micro nozzle used to control satellites altitude and trajectory exactly has become a research focus. As a kind of micro nozzle, free molecular micro-electro-thermal resist jet (FMMR) has developed very fast since 1980s. The configuration of a typical FMMR is shown in Fig. 1. The working principles of FMMR are as follows: the inlet propellant of low temperature flows over the heating surface, and the molecules of propellant knock with heating surface. After the collision, macroscopically the temperature of propellant raises which means that the microscopic velocity of molecules increases. Then the propellant rushes out of the nozzle with high speed and thrust is generated. For the purpose of enlarging collision rate between molecules and the heating surface while reducing collision rate between molecules, the dimension of nozzle should be in the order of the mean free path of the propellant molecules so that the rarefaction effect in the nozzle flow field becomes significant.

The degree of rarefaction for gas is usually expressed by Knudsen number (Kn), which in some sense represents the ratio of collisions between gas molecules and solid surfaces and collisions between gas molecules. Based on Kn, gas flow is classified into four regimes (Tsien 1946):

$Kn < 0.001$: continuum flow
$0.001 < Kn < 0.1$: slip flow
$0.1 < Kn < 10$: transition flow
$Kn > 10$: free molecule flow.

Usually the Knudsen number at the nozzle is >0.1 and the flow at the nozzle falls within the scope of transition flow or free molecule flow. Navier–Stokes equation based

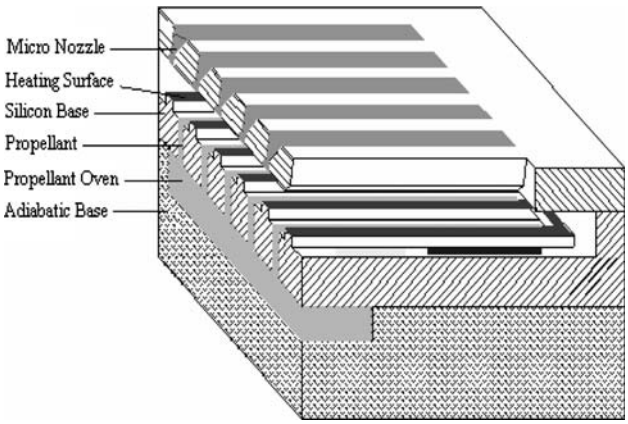

Fig. 1 Configuration of FMMR

on continuum assumption is valid in the continuum flow and it is also valid in the slip flow regime by resorting to slip boundary conditions. But it becomes invalid in the transition and free molecule regime. DSMC method developed by Bird (1994) is the most useful method to simulate the flow field in these regimes, and it is adopted here to predict the flow field in the FMMR shown in Fig. 1.

A large number of researches have been conducted for FMMR both experimentally and numerically. A number of authors have studied the flow field characteristics in the micro-nozzle with DSMC method. Wong et al. (2003) numerically studied the effect of thermophysical properties on the performance of FMMR. And a design of the heater chip of the next generation was proposed. Ahmed et al. (2005) numerically simulated the free molecule flow in different part of a micro-resisto jet in order, including the plume outside the vehicle, and compared their result with experimental data. In (Gimelshein et al. 2005) both experimental and numerical studies were conducted for rarefied gas flows through orifices and short tubes. Alexeenko et al. (2005, 2006) developed coupled thermal-fluid methods to simulate the time-dependent performance of high temperature micro-nozzle. In (Liu et al. 2006) the flow field of short tube by both DSMC and continuum method are predicted and then compared with experimental data. The results indicate that numerical simulation is in good agreement with experimental data, and with the increase of Kn the continuum method gradually becomes ineffective. In their study the threshold is taken about $Kn = 0.045$. Lilly et al. (2006) measured the mass flow and computed momentum flux of rarefied gases through short tubes. Xie (2007) expounded the phenomenon of multiple expansion-compression waves in the nozzle's divergent part. In most numerical simulations mentioned above the surface temperature of the nozzle wall was set up before calculation and assumed that it was constant during the simulation process. But in fact, the complicated structure of FMMR made it very difficult to set up wall temperature reasonably prior to computation. Alexeenko et al. (2005, 2006) developed coupled thermal-fluid methods to simulate the time-dependent performance of high temperature micro-nozzle. In their articles, the flow field characteristics were obtained by DSMC method and the solid area temperature distribution was calculated by finite element method. Dirichlet–Neumann transfer method was used to couple the temperature obtained by FEM and heat flux obtained by DSMC method at the boundary. The whole unsteady process from starting up to temperature reaching melting point of silicon was simulated, so it was very time-consuming and computationally expensive.

The present paper conducts a DSMC–FVM coupled simulation for the rarefied gas flow in a FMMR. The temperature of solid area is calculated with the finite volume method (FVM) based on energy equation and the field of flow area is simulated by DSMC method. An over-relaxation method is used in the unsteady solution process of heat conduction in the nozzle solid wall and hence the steady state is reached with a great time-saving. The temperatures of solid area and flow area are coupled together at the solid-fluid interface. An unstructured mesh is used for both the solid and fluid regions to meet the requirement of irregular domain of the gas flow.

In the following the numerical method will first be briefly presented followed by the validation for the developed code. Then simulated results for five cases with different inlet parameters are provided. The necessity of the couple method is also discussed. Finally some conclusions are made.

2 Numerical method

The propellant used is Argon and the variable hard sphere (VHS) model (Bird 1994) is used in this simulation. As shown in Fig. 1 several micro-nozzles are connected in parallel to increase the thrust and each nozzle can be regarded identical. Thus only one nozzle is adopted for simulation. The cross section dimensions of the nozzle are much less than the axial length; hence a 2D model is adopted in this paper as shown in Fig. 2. The fluid flow and heat transfer can be regarded symmetry about the nozzle axis, so only half of the cross section is used for computation. The structure of the nozzle cross section is quite complex so unstructured grid system is utilized in this simulation to perfectly simulate the tilted solid wall of the nozzle. Triangle is the basic cell in two dimensional unstructured grid systems and is adopted in this paper. The unstructured grid system adopted in the computation is shown in Fig. 3.

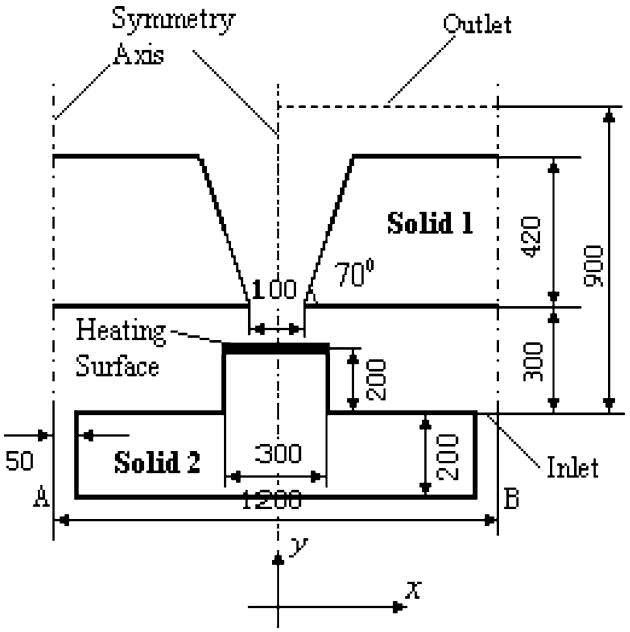

Fig. 2 Details of a cross-section configuration of FMMR

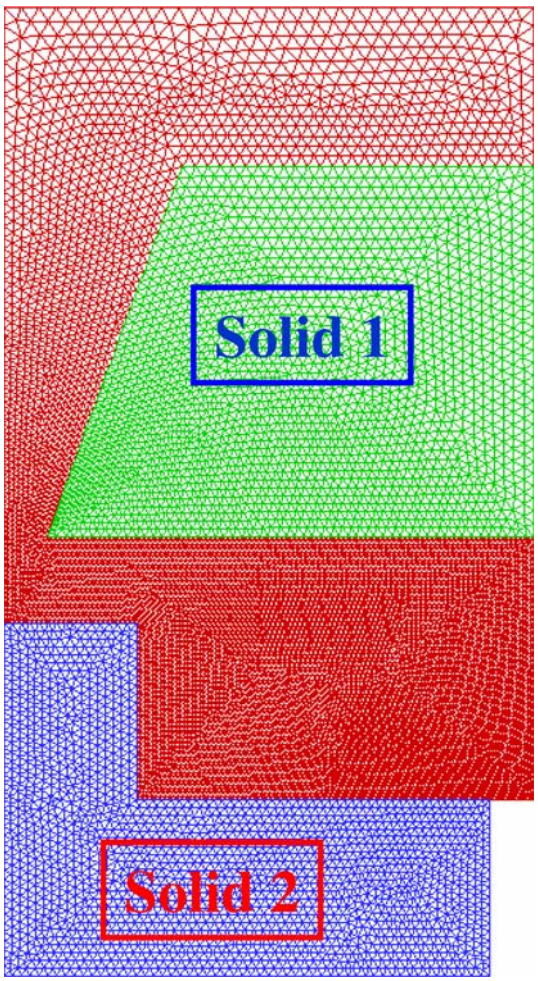

Fig. 3 The unstructured grid system

Mean free path is an important parameter in DSMC which means the average length of track between collisions, and it can be obtained by Eq. 1 (Bird, 1994).

$$\lambda = \frac{1}{\sqrt{2}\pi d^2 n}, \quad \text{where } n = \frac{P}{kT} \tag{1}$$

where d is the molecule diameter and k is the Boltzmann constant.

Then the mean free time is

$$\Delta t = \lambda / v \tag{2}$$

$$v = \sqrt{2kT/m}$$

where v is the most probable molecular speed and m is the molecular mass.

The Knudsen number is the ratio of the mean free path over a characteristic length and for the nozzle studied, and it is determined as follows

$$Kn = \frac{\lambda}{L} = \frac{1}{\sqrt{2}\pi d^2 nL} \tag{3}$$

where L is the characteristic length and is taken as the width of the nozzle throat.

In order to obtain accurate results by DSMC, the cell dimensions should be less than the mean free path (Alexander et al. 1998, 2000) and the time step must be less than mean free time between two collisions (Nicolas and Hadjiconstantinou 2000). As for the appropriate number of particles placed in a cell, different opinions still exist. The principle proposed by Bird (2007) indicates that 7 is the optimum number and if the number exceeds 7, the error is very small but if lower than 7, the error may become larger.

For the purpose of ensuring a molecule collide with molecules nearby, a triangular cell may be further divided into sub-cells. By linking three midpoints of edges a cell is then divided into four sub-cells (Fig. 4). It can be imagined that the pressure in the flow field decreases gradually from the inlet to the outlet, which means that the number density of molecules decreases from inlet to outlet while mean free path of molecules increases in this process (Eq. 1). According to the above characteristics, the grid system with increasing grid dimension along flow direction is adopted in this simulation (Fig. 5), so the number of

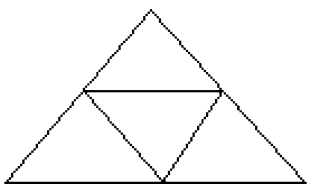

Fig. 4 A cell divided into four sub-cells

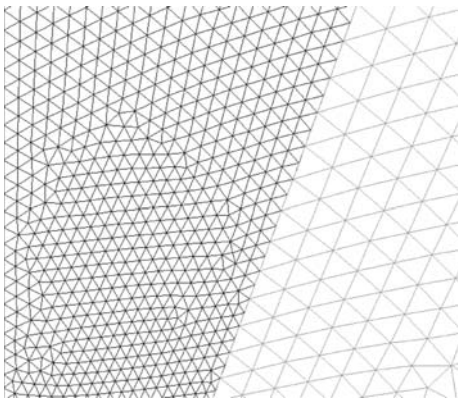

Fig. 5 Grid system with increasing grid dimension

molecules in each cell will be approximately constant. Even though the number of particles per cell is not constant exactly within the flow field, the minimum number of particles per cell is greater than 5. In the figure the left part is the flow field grid with the increasing grid dimension while the right part is the grid of solid 1. The cell dimension, the number of molecules per cell and the time step are all set up in accordance with the above-mentioned principle.

Attention is now turned to the boundary condition set up (see Fig. 2). The so-called "pressure boundary condition", that is the inlet pressure, inlet temperature and outlet pressure are set up before calculation, is usually used in DSMC simulation, and this condition is adopted in the present simulation. The method proposed by Liou and Fang (2000) and improved by Wang and Li (2004) suggested that statistical macroscopic velocity obtained from particle in the cells near the inlet boundary can be used as the income velocity for new particles. These methods are adopted in this paper. Other parameters are determined in the following way at inlet boundary:

$$(U_{\text{in}})_j = U_j + \frac{P_{\text{in}} - P_j}{\rho_j a_j} \tag{4}$$

$$(V_{\text{in}})_j = V_j \tag{5}$$

$$n_{\text{in}} = \frac{P_{\text{in}}}{kT_{\text{in}}} \tag{6}$$

Similarly, parameters except pressure at outlet boundary are determined as follows:

$$(U_{\text{e}})_j = U_j + \frac{P_j - P_{\text{e}}}{\rho_j a_j} \tag{7}$$

$$(V_{\text{e}})_j = V_j \tag{8}$$

$$(\rho_{\text{e}})_j = \rho_j + \frac{P_{\text{e}} - P_j}{(a_j)^2} \tag{9}$$

$$(T_{\text{e}})_j = \frac{P_{\text{e}}}{(\rho_{\text{e}})_j R} \tag{10}$$

$$n_{\text{e}} = \frac{\rho_{\text{e}}}{m} \tag{11}$$

In the above equations, the symbols without brackets are the macroscopic parameters obtained from the cell near the boundary while the symbols with brackets are the parameters assigned to particles that just come into the computational field.

The FMMR is working in vacuum environment so the outlet pressure of all the simulated cases is zero.

The lower surface and right surface in the lower part of solid 2 (see Fig. 3) are parts of a reservoir boundary within which the propellant is stored. For the purpose of saving energy, some thermal insulation material layer is fixed outside the reservoir surface, so the thermal insulation boundary condition is utilized along the two surfaces.

The other two boundaries, as shown in Fig. 2, are both symmetric. The treatment of the interface condition between fluid and solid wall will be presented later.

3 Code verification

The developed DSMC code of unstructured grid is verified by comparing the Poiseuille flow result obtained by our code with the results from the code of rectangular gird developed by Bird and the analytical result of Arkilic et al. (1997). The schematic of the channel flow is shown in Fig. 6. The dimensions of the flow field are set as 8 × 1 μm. The pressure boundary condition is utilized in this study. The income pressure P_{in} and temperature T_{in} are set at 1.2 atm and 300 K, respectively. The exit pressure P_{e} is 0.5 atm and the temperature of the wall is set just the same as the income temperature. Advancing front method is used to discretize the flow domain with unstructured grid of triangle. The Knudsen number is 0.045 at the entrance area and 0.10 at the exit area, so the flow field should be classified in slip flow regime. Diffuse reflection model (Bird 1994) is used as the surface–molecule interaction model in this verification.

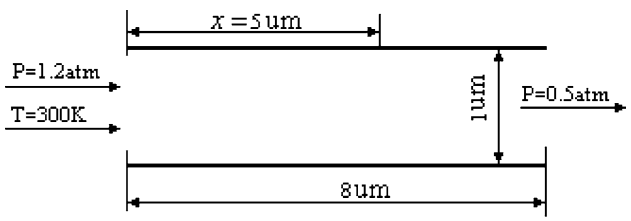

Fig. 6 Schematic of Poiseuille flow for code verification

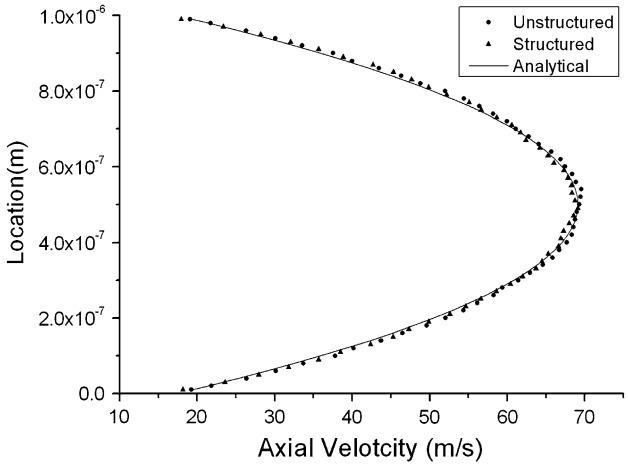

Fig. 7 Cross-section velocity at $x = 5$ μm

The mean free path of the molecules in the entrance region is the smallest within the flow field and value is 44.1 nm. The side length of triangular grid is 20 nm which is less than half of mean free path, and the whole flow field is decomposed into 45,226 cells. The mean free time between collisions in the entrance is also the smallest and its value is 1.2×10^{-10} s. The time step in this calculation is 1.5×10^{-11} s which equals to one-third of the time of a molecule crossing a triangle grid. The number density at the exit region is the least within the flow field, and the number of particles per cell in this area is 18 which is still greater than 7. From the parameters shown above we can conclude that the grid system, time step and the number of particles per cell used in this verification are reasonable.

Figure 7 shows the axial velocity at the cross-section of $x = 5$ μm calculated by the program with triangular cell, rectangular cell of Bird (1994) and analytical solution of Arkilic et al. (1997). From the comparison we can come to the conclusion that the developed DSMC code with the unstructured grid system used in this simulation is reliable.

4 Parameters and coupling of FMMR simulation

The working conditions used in this simulation are listed in Table 1. Propellant with the temperature of 300 K enters flow field from the reservoir and then is heated when it flows over the heating surface (Fig. 2). The temperature of heating surface is 600 K. Cercignani–Lampis–Lord (CLL) model (Bird 1994) is used to simulate the interaction between the solid surface and molecules and the accommodation coefficient is set as 0.73. The material of solid area is silicon with the thermal conductivity of 149 W/(m K). The flow field is divided into 16,696 grids for Cases 1, 2 and 3, 26,792 grids for Case 4 and 45,720 grids for Case 5.

Table 1 Working conditions used in this simulation

Case	1	2	3	4	5
Inlet pressure (Pa)	500	1,000	2,000	5,000	10,000
Outlet pressure (Pa)	0	0	0	0	0
Inlet temperature (K)	300	300	300	300	300

The boundary condition coupling at the fluid–solid interface is now described. The Dirichlet boundary conditions, namely, the surface temperature has to be pre-set before DSMC process for the fluid region and the Neumann boundary condition, i.e., the flux at the surface can be obtain from the DSMC simulation. This heat flux is then used as the input at the interface for the solid wall heat conduction simulation. Such Dirichlet–Neumann transferring method is used to couple the temperature and heat flux at the boundary of flow field and solid area. The implementation process is as follows. First the wall surface temperature is set up and then DSMC simulation is executed, so the heat flux can be calculated from the flow field, and this heat flux is used as the boundary condition for the temperature field of the solid area including the wall surface. The temperature field in the solid area is obtained by solving the heat conduction equation with the FVM on the unstructured grid system. The wall surface temperatures are thus updated and used as the boundary condition for the flow field solved by DSMC. Such steps are repeated until steady state has reached. Once steady state has reached, the solid temperature will not be calculated any more, namely, the surface temperature of fluid area is kept constant, but DSMC procedure in the fluid is continued. The sampling of macro-parameters with each cell should be performed for a long time period in order to minimize statistical scatter. The details of the boundary conditions of solid 1 are now addressed. The left, upper and lower surfaces of solid 1 are in contact with gas and the Dirichlet–Neumann transferring method mentioned above is used for the three boundaries. The right surface of solid 1 is of symmetry type. Thus all the four boundaries of solid 1 is of second kind. It is well-known in heat conduction theory that such boundary conditions will lead to a temperature distribution with fixed gradient but can not fix the absolute values. The energy conservation principle is used to fix the temperature distribution of solid 1, namely, when the converged temperature solution of solid 1 is approached, the net heat transfer of solid 1 with the gas around it should be zero.

Due to the low density of the propellant, the heat flux is very small, so there is little temperature change in solid area during every time step. It would take a long time to arrive at steady state which means that the time-marching of the unsteady state process in solids is computationally

expensive. Considering that the time scale of flow area is much less than the time scale of solid area, namely, the time spent during the fluid area unsteady process is much less than the time spent during the solid area unsteady process (Alexeenko et al. 2005, 2006), a steady-state solution of gas flow is first obtained and the DSMC results are used to update the wall boundary condition. An over-relaxation method is adopted in the solution process of heat conduction equation that accelerates the convergence but does not influence the steady state temperature distribution in the solid region.

5 Results and discussion

Figure 8 shows the stream lines of the flow field for Case 3. As expected, propellant comes into the field from inlet and then flows through the throat. Such general flow picture is the same for all the five cases studied, and only the result of Case 3 is presented for simplicity.

Figure 9 shows the temperature distribution in solid 1. We can see that the temperature near heating surface is a bit higher due to the impact of nearby gas with both high temperature and high density. The temperature in the area near the propellant entrance is relatively low because the gas of low temperature knocked with surface. From temperature distribution we can conclude that heat conducted from area near heating surface to area near entrance to heat up propellant, even though very weak. Although propellant temperature above solid 1 is low, due to the relatively low density, there is only a very little heat flux transferred from solid 1 to fluid, so the isothermal lines in solid 1 are nearly normal to the top surface. Figure 10 shows the temperature distribution of solid 2. The left side of upper surface is the heating surface with the temperature of 600 K and the surfaces at base, left side and lower part of right side are adiabatic. Just as the case of solid 1, heat also conducted very weakly from heating surface to area near entrance to heat up propellant.

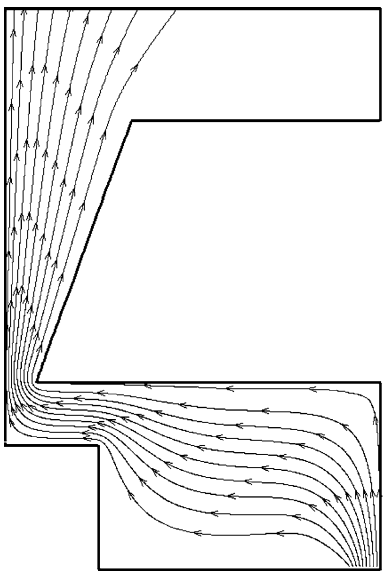

Fig. 8 Stream lines of flow field (Case 3)

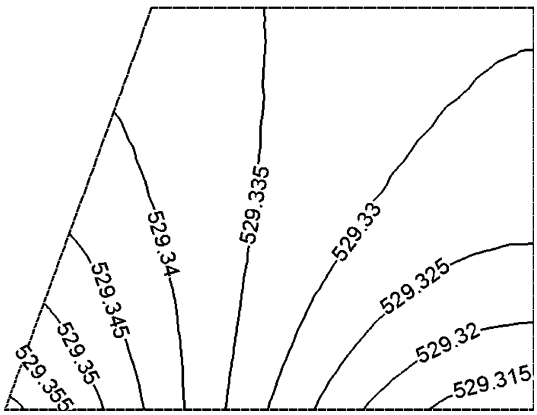

Fig. 9 Temperature distribution of solid 1 (Case 3, K)

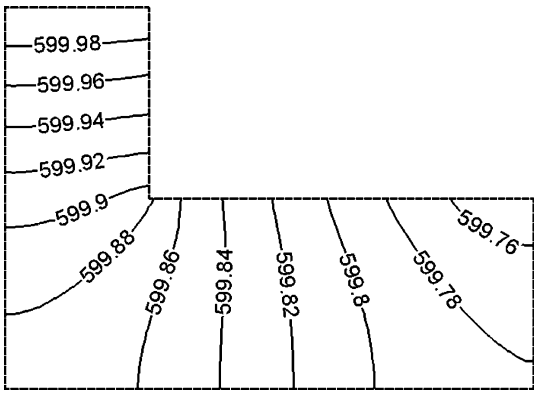

Fig. 10 Temperature distribution of solid 2 (Case 3, K)

From the temperature distribution in the two solid areas we can conclude that the temperature difference within the solid region is very small due to low density of the propellant and high thermal conductivity of silicon. So a "general temperature" may be assumed for each solid areas. For example, the temperature difference between maximum and minimum of solid 2 is less than 0.2 K, and that in solid 1 even less than 0.1 K. So the general temperature of solids 1 and 2 for Case 3 can be set as 529 and 600 K, respectively. Table 2 presents the general temperature of solid 1 under different work conditions. As can be seen from the table that the temperature changes drastically under the same heating surface temperature but different inlet pressure, and the general temperature decreases with the increase of pressure. Such results are very different from the general idea of "The higher the pressure; the

Table 2 Performance parameters of FMMR

Case	Inlet pressure (Pa)	Throat pressure (Pa)	Throat Knudsen number	Throat velocity (m/s)	Throat (Ma)	Throat (Re)	Solid 1 temperature (K)	Mass flow rate (kg/s)	Thrust (N)	Specific impulse (s)
1	500	218	0.52	218	0.51	1.2	567	2.22E-05	0.013	58
2	1,000	459	0.25	237	0.56	2.8	561	5.09E-05	0.030	59
3	2,000	974	0.11	257	0.62	7.1	529	1.23E-04	0.073	61
4	5,000	2,802	0.031	262	0.68	27.6	433	4.18E-04	0.25	61
5	10,000	6,572	0.012	262	0.71	72.5	423	1.02E-03	0.63	63

higher the temperature". The variation of the solid general temperature with the inlet pressure may be explained as follows: As the pressure increase, the mean free path of molecules decreases, namely, the value of *Kn* decreases, so the molecules just leave the heating surface with high velocity knock with other molecules more frequently and then the ratio of molecules knocking at solid 1 decreases, leading to the reduction of wall temperature. It is worth noting that although the temperature difference within solid 1 is negligible, it is still necessary to solve the energy equation of solid 1. The reason is as follows. The temperature uniformity of the solid region is the outcome of the coupled solution of solid heat conduction and the gas flow in the nozzle. We have no way to prescribe some temperature level for the solid region for different conditions a priori. Furthermore it is only by such coupled simulation that we can reveal the variation trend of the solid wall temperature with the inlet gas pressure.

Figure 11 shows the temperature distributions in flow field. From the five isothermal contours following general features may be noted. (1) Along the flow path the fluid temperature increases first due to the heat transfer between solid area and propellant, then decreases sharply in the region of the nozzle throat, and at the nozzle exit the fluid temperature reduces to the lowest value. (2) In the nozzle region at the same cross section because of the viscous effect, the temperature near the nozzle wall is higher than that near the symmetry axis. (3) At the low inlet pressure condition the isothermal orientations are more or less normal to the fluid flow direction, while at the high inlet pressure, the isothermals move towards the orientation of parallel to the fluid flow direction, which is a basic characteristics of the continuum fluid flow, characterized by the isotherms in boundary layer flow in the continuum mechanics. This feature may be viewed from another point: with the increase of inlet pressure, the influence of income parameter increases and the influence of heating surface decreases.

Figure 12 shows pressure distribution in flow field of Case 3. From the figure we can see that the change is not obvious from inlet to the throat of the nozzle but become drastic near the throat because of velocity increase and channel expansion. After the nozzle, the pressure decreases further and reaches the minimum above solid 1.

Figure 13 shows density distribution in flow field of Case 3. Unlike the pressure distribution, the density changes obviously both in the area near the entrance and the area in the throat. After the nozzle, the density decreases further and reaches the minimum above solid 1. The difference between pressure and density distributions in the region ahead of the throat can be explained as follows: The propellant temperature increases sharply after entering into the domain. From the equation $P = nkT$ we can see that with the increase of temperature, the density decreases under the condition of nearly constant pressure.

Figure 14 shows Mach number distribution in the flow field. The propellant velocity increases after the throat and reaches maximum after the nozzle. In Case 1, the propellant exceeds sonic velocity after a certain distance off the throat which is different from the nozzle flow in the continuum regime. With the increase of income pressure, the distance (between throat and the point that propellant velocity surpassed sonic velocity) becomes smaller. The maximum Mach number of the whole flow field and the velocity gradient near the wall surface also increase as the increase of the inlet pressure.

Figure 15 shows the transverse velocity distribution in flow field of Case 3. The transverse velocity reaches 350 m/s after the nozzle in the area above solid 1. Such high speed reduces the efficiency so the structure of nozzle may be improved to cut down the transverse velocity.

Table 2 presents the performance parameter of the nozzle. The thrust and specific impulse are obtained by the following equations:

$$F_{\mathrm{t}} = \int (\rho_{\mathrm{e}} u_{\mathrm{e}}^2 + P_{\mathrm{e}}) h_{\mathrm{e}} \mathrm{d}y \tag{12}$$

$$I_{\mathrm{sp}} = F_{\mathrm{t}}/(\dot{m}g) \tag{13}$$

From Table 2 we can conclude that different parameter changes in a different way with the inlet pressure. Throat pressure changes almost the same way as the inlet pressure while the Reynolds number at throat, the mass flow rate

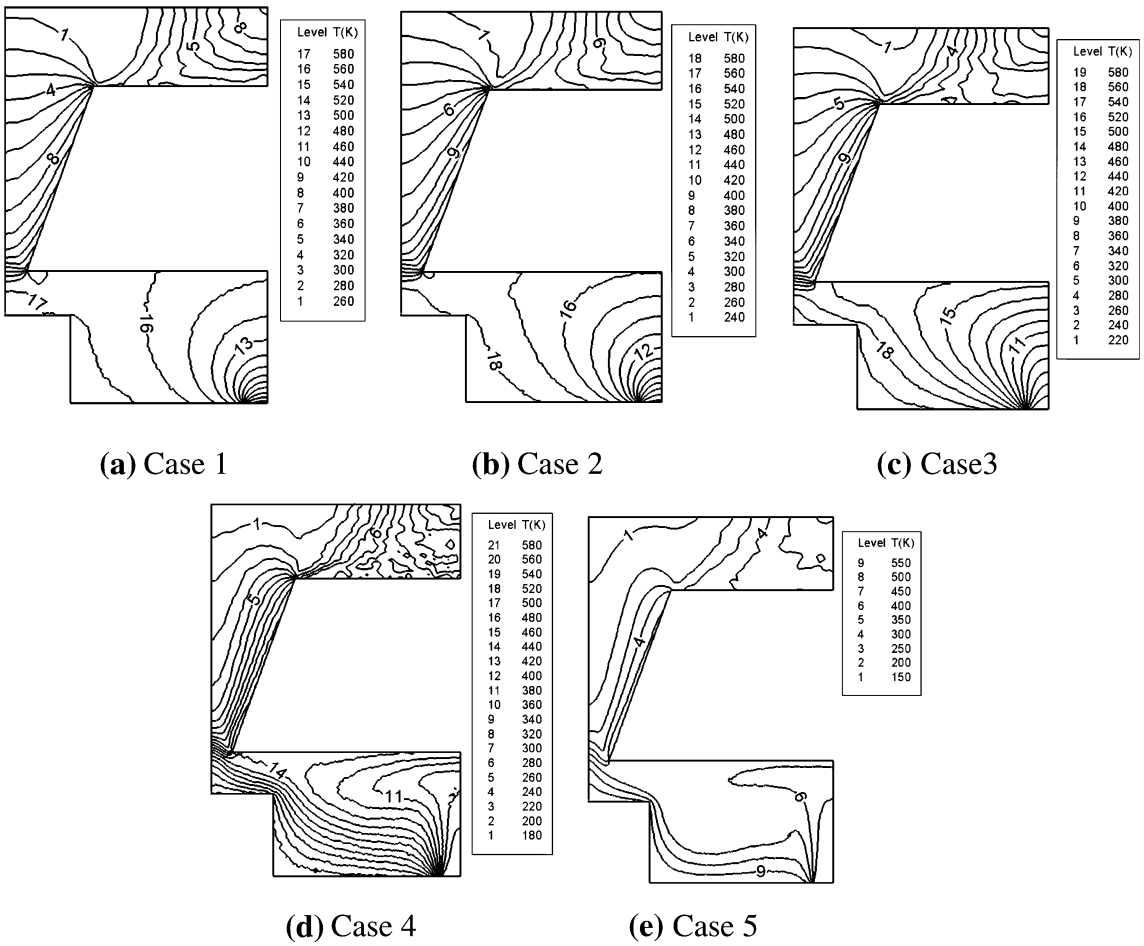

Fig. 11 Temperature distribution

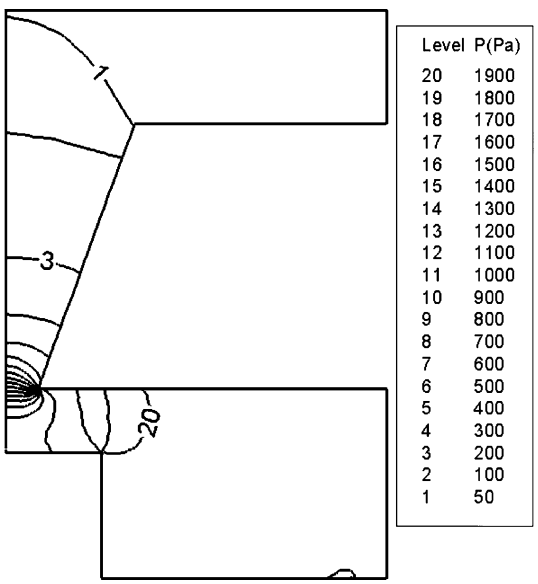

Fig. 12 Pressure distribution (Case 3)

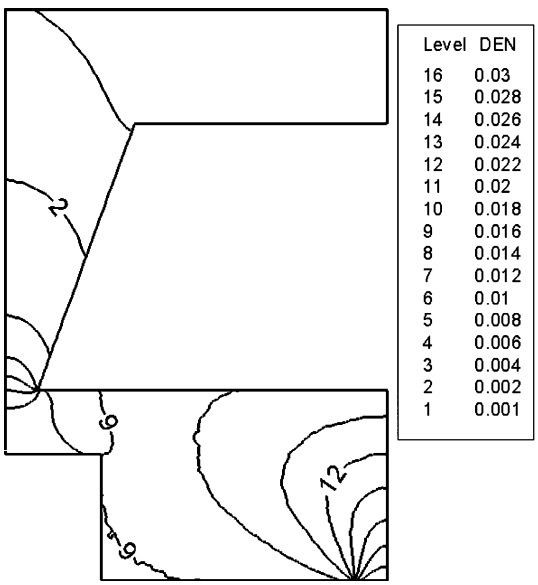

Fig. 13 Density distribution (Case 3, kg/m^3)

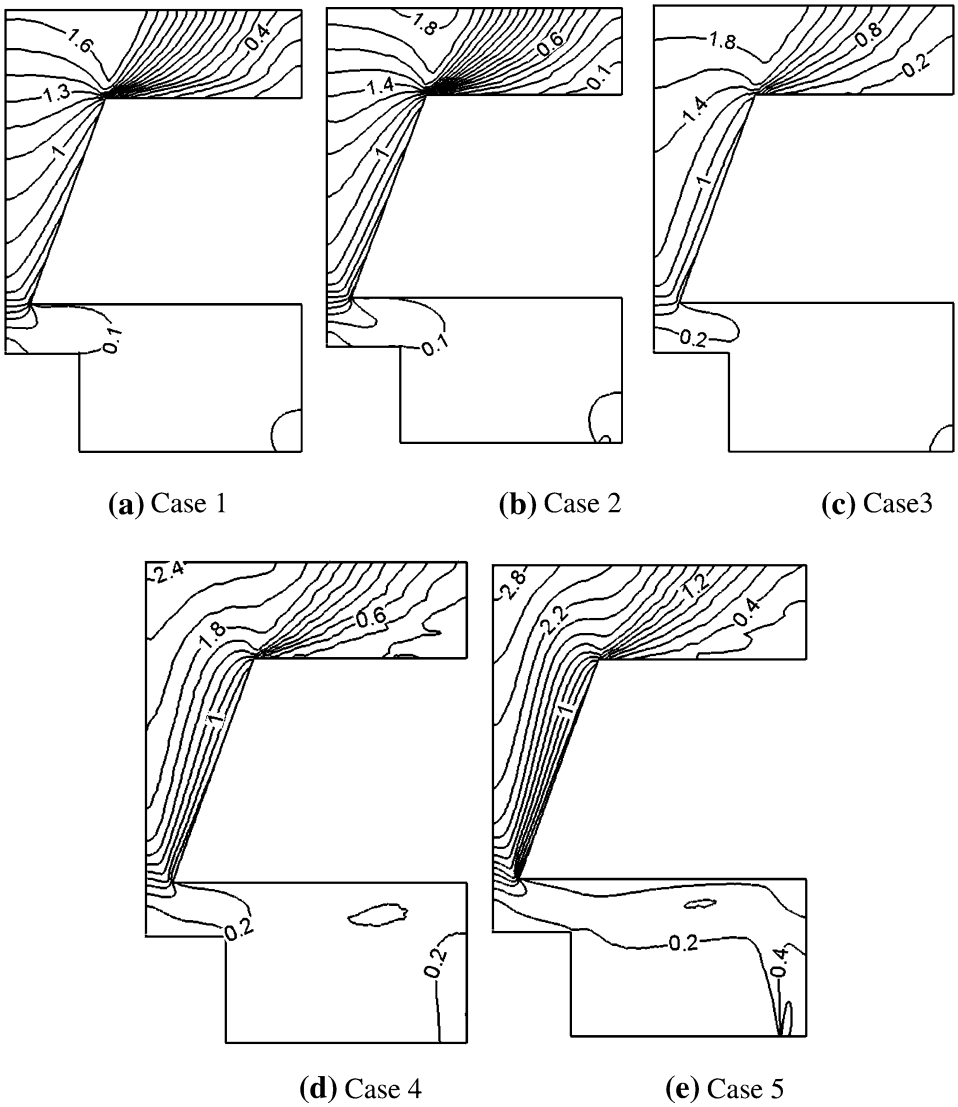

Fig. 14 Mach number distribution

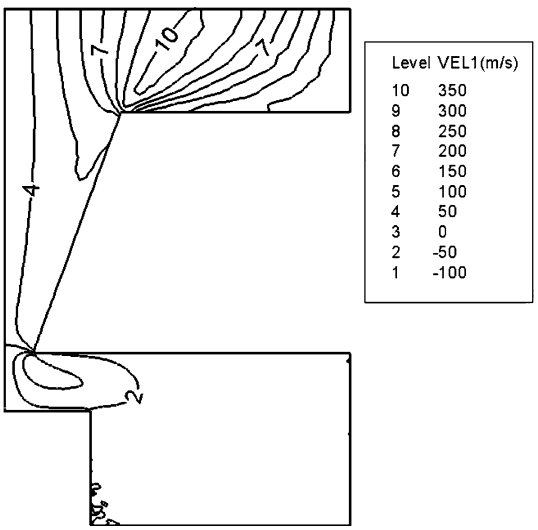

Fig. 15 Transverse velocity distribution (Case 3)

and thrust change much rapidly than the pressure. The thrust is virtually directly proportional to Reynolds number at throat, so the propulsion performance of micro nozzle can be considered as a function of Reynolds number at the throat (Liu et al. 2006). The specific impulse is kept almost constant under different working conditions. The thrust specific impulse is a kind of nozzle efficiency as defined by Eq. (13). The almost constant specific impulse is beneficial to the micro satellite control because the nozzle efficiency is almost kept constant within a wide variation range of the thrust.

For the purpose of evaluating the necessity of DSMC–FVM coupled method, additional computation was conducted for cases by pre-setting the temperature of solid area and keeping constant during process. The results are listed in Table 3 where Case A1 to A3 have the same inlet pressure as Case 3 of Table 1 while the solid 1 temperature was pre-specified and kept as 450, 529, and 600 K, respectively.

Table 3 Performance parameters of FMMR for additional calculation

Case	Inlet pressure (Pa)	Throat pressure (Pa)	Throat Knudsen number	Throat velocity (m/s)	Throat (Ma)	Throat (Re)	Solid 1 temperature (K)	Mass flow rate (kg/s)	Thrust (N)	Specific impulse (s)
A1	2,000	1,001	0.096	252	0.63	8.2	450	1.34E-04	0.076	58.0
A2	2,000	974	0.11	257	0.62	7.1	529	1.23E-04	0.073	60.6
A3	2,000	976	0.12	263	0.61	6.4	600	1.17E-04	0.072	62.8

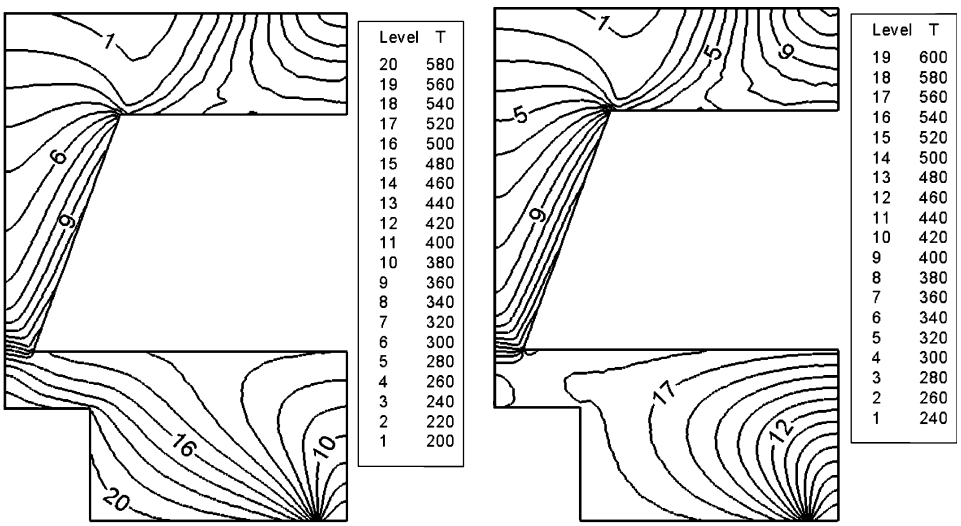

Fig. 16 Fluid temperature distributions from computations with pre-specified wall temperature

(a) Case A1 **(b)** Case A 3

From the comparison we can observe that the specific impulse increases as the increase of solid 1 temperature but the mass flow rate and thrust decreases. Figure 16 shows the temperature distribution of the flow field for Cases A1 and A3. By comparing with Fig. 11c we can conclude that the fluid temperature distributions of Cases A1 and A3 are obviously different from Case 3, and so are other major results of computations, including the mass flow rate, and the specific impulse. Thus the pre-specified wall temperature method is not feasible and the DSMC–FVM coupled simulation is necessary for low temperature micro nozzle.

6 Conclusions

In this paper the coupled simulation by DSMC for gas flow in the slip and transition regimes and the temperature of solid in the continuum region by FVM are conducted for a FMMR. Following conclusions may be drawn. The temperature difference within solid area of micro nozzle was very small, so a "general temperature" or an average temperature may be assumed in the solid area. However, the general temperature of solid 1 changes drastically under different working conditions, so DSMC–FVM coupled method is compulsory for FMMR simulation. As the increase of income pressure, the distance between throat and the point that propellant velocity surpassed sonic velocity becomes smaller. Notable difference exists between the density and pressure distribution in the flow field due to the increase of temperature. The specific impulse is kept almost constant under different working conditions which is meant that nozzle efficiency is kept at high level although the thrust changes.

Acknowledgments The present work was supported by the National Natural Science Foundation of China (50636050) and the Foundation for Authors of National Excellent Doctoral Dissertation of China (No. 200436).

References

Ahmed Z, Gimelshein S, Ketsdever A (2005) Numerical analysis of free molecule micro-resistojet performance. AIAA Paper 2005-4262

Alexander F, Garcia A, Alder B (1998) Cell size dependence of transport coefficients in stochastic particle algorithms. Phys Fluids 10(6):1540–1542

Alexander F, Garcia A, Alder B (2000) Erratum: "cell size dependence of transport coefficients in stochastic particle algorithms". Phys Fluids 12(3):731

Alexeenko A, Levin D, Fedosov D, Gimelshein G (2005) Performance analysis of microthrusters based on coupled thermal-fluid modeling and simulation. J Propuls Power 21(1):95–101

Alexeenko A, Fedosov D, Gimelshein S, Levin D, Collins R (2006) Transient heat transfer and gas flow in a MEMS-based thruster. J Microelectromech Syst 15(1):181–194

Arkilic A, Schmidt M, Breuer K (1997) Gaseous slip flow in long microchannels. J Microelectromech Syst 6(2):167–178

Bird G (1994) Molecular gas dynamics and the direct simulation of gas flows. Clarendon Press, Oxford

Bird G (2007) Sophisticated DSMC, Notes prepared for a short course at the DSMC07 meeting Santa Fe, September 30, 2007

Gimelshein S, Markelov G, Lilly T, Selden N, Ketsdever A (2005) Experimental and numerical modeling of rarefied gas flows through orifices and short tubes. In: 24th international symposium on rarefied gas dynamics, pp 437–443

Lilly T, Gimelshein S, Ketsdever A, Markelov G (2006) Measurements and computations of mass flow and momentum flux through short tubes in rarefied gases. Phys Fluids 18:093601

Liou W, Fang Y (2000) Implicit boundary conditions for direct simulation Monte Carlo method in MEMS flow predictions. Comput Model Eng Sci 1(4):119–128

Liu M, Zhang X, Zhang G, Chen Y (2006) Study on micronozzle flow and propulsion performance using DSMC and continuum methods. Acta Mech Sin 22:409–416

Nicolas G, Hadjiconstantinou NG (2000) Analysis of discretization in the direct simulation Monte Carlo. Phys Fluids 12(10):2634–2638

Tsien H (1946) Superaerodynamics, the mechanics of rarefied gas. J Aeronaut Sci 13:653–664

Wang M, Li Z (2004) Simulations for gas flows in microgeometries using the direct simulation Monte Carlo method. Int J Heat Fluid Flow 25:975–985

Wong J, Ketsdever A, Reed H (2003) Numerical modeling of the free molecule micro-resistojet prototype and next generation designs evaluation. AIAA Paper 2003-3581

Xie C (2007) Characteristics of micronozzle gas flows. Phys Fluids 19:037102